Materials Chemistry and Physics 250 (2020) 122954

Contents lists available at ScienceDirect

Materials Chemistry and Physics

journal homepage: www.elsevier.com/locate/matchemphys

Crystal structure, Raman spectroscopy, metal compatibility and microwave dielectric properties of $Ce_2Zr_3(MoO_4)_9$ ceramics

Liang Shi [a], Cheng Liu [a,b,*], Huaiwu Zhang [a,b], Rui Peng [a], Gang Wang [a], Xiaolei Shi [a], Xueying Wang [a], Wenwen Wang [a]

[a] School of Electronic Science and Engineering, University of Electronic Science and Technology of China, Chengdu, 610054, China
[b] State Key Laboratory of Electronic Thin Films and Integrated Devices, University of Electronic Science and Technology of China, Chengdu, 610054, China

GRAPHICAL ABSTRACT

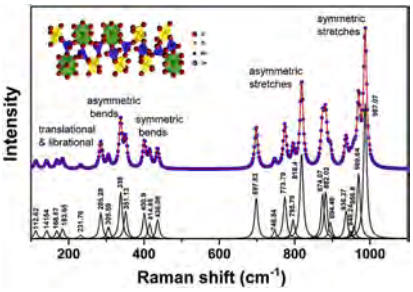

ARTICLE INFO

Keywords:
$Ce_2Zr_3(MoO_4)_9$ ceramics
Raman spectroscopy
Crystal structure

ABSTRACT

Low temperature sintered $Ce_2Zr_3(MoO_4)_9$ ceramics were synthesized via the conventional solid-state reaction method. Microstructure and microwave dielectric properties were systematically investigated via the assistance of Raman spectroscopy. Pure phase of $Ce_2Zr_3(MoO_4)_9$ with R–3C space group were obtained, as confirmed through the XRD and Rietveld refinement results. The Raman spectroscopy results indicated that the Raman-active vibrations are mainly derived from the Mo–O bonds. The SEM images exhibited that the porosity and grain morphology, as external factors, affected the microwave dielectric properties, along with the internal factors, such as packing fraction. In addition, theτ_f values were inversely affected by the distortion of the Zr–O polyhedron. The sample sintered at 750 °C exhibited good microwave dielectric properties: $\varepsilon_r = 10.05$, $Q \times f =$ 24,720 GHz (at 11.3 GHz) and $\tau_f =$ -7.1 ppm/°C. The compatibility between $Ce_2Zr_3(MoO_4)_9$ ceramic matrix and silver/copper electrode was also investigated for the first time.

1. Introduction

The rapid development of wireless communication requires small, lightweight, and multifunctional electronic devices for antenna, filter, and resonator applications. As one of the effective solutions, low temperature co-firing ceramics (LTCC) technology is developed for device miniaturization and integration. Exploring more suitable microwave dielectric materials sintered with metal electrode compatible for these multifunctional electronic devices attracts much attention [1–4]. However, low dielectric loss, thermal-stable, and metal-compatible

* Corresponding author. School of Electronic Science and Engineering, University of Electronic Science and Technology of China, Chengdu, 610054, China.
E-mail address: c_liu@uestc.edu.cn (C. Liu).

https://doi.org/10.1016/j.matchemphys.2020.122954
Received 4 December 2019; Received in revised form 18 March 2020; Accepted 20 March 2020
Available online 7 April 2020
0254-0584/

dielectric matrix are requested for LTCC technology. In general, silver (Ag) and copper (Cu) are widely used as the internal electrodes due to their high conductivity and low cost, but melting point of Ag is only about 960 °C [5–8]. Therefore, it is essential to lower the sintering temperature of the dielectric ceramics less than 960 °C to meet the co-firing compatibility between the ceramic matrix and the silver or copper electrodes [9]. Normally, glasses and oxides with low melting points are usually adopted to lower the sintering temperature, but the formation of secondary phases deteriorates the microwave dielectric properties [10]. Therefore, new types of microwave dielectric ceramics with promising LTCC characteristics are of great significant.

Recently, monophasic oxide ceramics with low sintering temperature, such as molybdate, bismuth, and vanadate have been studied extensively [11]. Pang et al. reported good microwave dielectric properties in $Ln_2Mo_3O_{12}$(Ln = La, Nd) ceramics: $\varepsilon_r = 10.1$, $Q \times f = 60{,}000$ GHz, and $\tau_f = -80$ ppm/°C with a sintering temperature of 930 °C for 2h [12]. Liu and Zuo uncovered that the $La_2Zr_3(MoO_4)_9$ system also exhibited good microwave dielectric properties: $\varepsilon_r = 10.8$, $Q \times f = 50$, 628 GHz (at 10.45 GHz), and $\tau_f = -38.8$ ppm/°C (sintered at 775 °C for 4h) [13]. Latest discovery on $Ce_2Zr_3(MoO_4)_9$ ceramics reported good microwave dielectric performance and related chemical bond theory [14].

Generally, molybdate microwave dielectric ceramics have complex crystal structure, which is closely related to the microwave dielectric performance. Raman spectroscopy is usually adopted to investigate the short-range character. However, the effect of molecular vibration and rotation on dielectric properties of $Ce_2Zr_3(MoO_4)_9$ ceramics has not been reported. In this work, pure phase of $Ce_2Zr_3(MoO_4)_9$ ceramics with trigonal structure were explored. The sintering behaviors, microstructure, crystal structure, microwave dielectric properties, and metal compatibility were investigated systematically.

2. Experiment

$Ce_2Zr_3(MoO_4)_9$ ceramics were synthesized via reagent-grade starting materials of CeO_2, ZrO_2, and MoO_3 (all purity>99%, Aladdin Industrial Co, Shanghai, China). The reagent powders were weighed in molar ratio, ball milled and mixed with deionized water for 10 h. Then the slurry was dried and calcined at 650 °C for 4 h. After re-milling for another 10 h, the mixture powders were dried and grinded into fine particles with 5 wt % of polyvinyl alcohol (PVA), and pressed into cylindrical bulks with diameter of 12 mm and thickness of 6 mm under 10 Mpa. The bulks were placed in air and sintered at 700–775 °C for 4 h.

The phase structure was analyzed by X-ray diffraction (XRD: Philips X'pert Pro MPD, PANalytical Company, Almelo, Holland) using Cu-Kα radiation at a scanning rate of 10°/min within a detecting range of 10° - 80°. The microstructure of the as-sintered samples was observed by Scanning Electron Microscope (SEM: JEOL JSM-6490, Tokyo, Japan). The Raman spectra were detected by the Raman microscope (In Via, UK) and laser source (i = 532 nm) in the range of 100–1100 cm^{-1}. The microwave dielectric properties were measured through the Hakki-Coleman dielectric resonator method [15] with a network analyzer (Agilent N5230A, Agilent Technologies, USA). The temperature coefficient of resonant frequency value (TCF, τ_f) is calculated by the following equation:

$$\tau_f = \frac{f_T - f_{T0}}{(T - T_0) \times f_{T0}} \times 10^6 ppm \Big/ ^{\circ}C \quad (1)$$

Where f_T and f_{T0} correspond to the resonant frequencies at temperature T (85 °C) and T_0 (25 °C), respectively.

The apparent density was measured by the Archimedes drainage method. Compared with water, kerosene was adopted as the drainage medium due to its higher viscosity. The theoretical density and the relative density were calculated by the following equations:

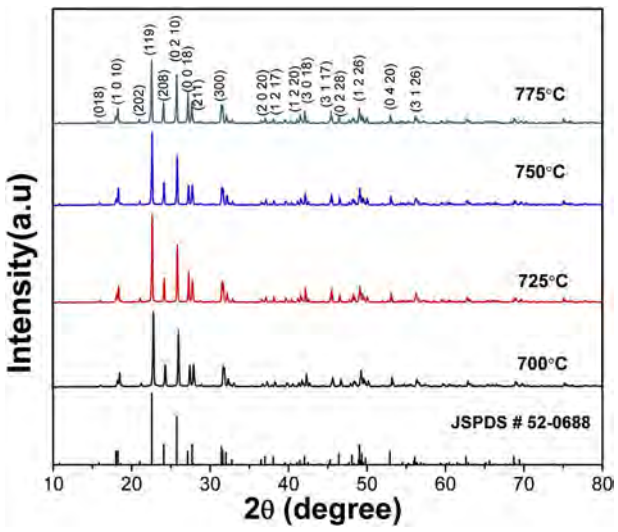

Fig. 1. XRD patterns of the $Ce_2Zr_3(MoO_4)_9$ ceramics sintered at different temperature.

$$\rho_{relative} = \frac{\rho_{measure}}{\rho_{theory}} \times 100\% \quad (2)$$

$$\rho_{theory} = \frac{MZ}{N_A V_C} \quad (3)$$

Where M, Z, N_A , and V_C represent the molar mass of unit cell, the number of formula units per unit cell, the Avogadro's number, and the volume of unit cell, respectively.

3. Results and discussion

Fig. 1 shows the XRD diffraction patterns of the $Ce_2Zr_3(MoO_4)_9$ ceramics sintered within the temperature range of 700–775 °C. All diffraction patterns match well with the phase structure of the $La_2Zr_3(MoO_4)_9$ ceramics (JSPDS # 52–0688) with R–3C space group, and no impure phases detected. Compared with the standard PDF card of JSPDS # 52–0688, all diffraction peaks of the $Ce_2Zr_3(MoO_4)_9$ ceramics locate at higher angles, which is due to the smaller ionic radius of Ce^{3+} (1.01 Å) than La^{3+} (1.07 Å) [16].

Fig. 2(a–d) exhibits the Rietveld refinement patterns of the $Ce_2Zr_3(MoO_4)_9$ ceramics sintered at different temperature, which are obtained via the GSAS software through a structural model of $Nd_2Zr_3(MoO_4)_9$ [17]. The calculated XRD diffraction pattern matches well with the actually measured, manifesting that the pure phase of $Ce_2Zr_3(MoO_4)_9$ ceramics are formed. Table 1 lists the lattice parameters, unit cell volumes, and reliability factors (Rwp: reliability factor of the patterns, Rp: reliability factor of the weighted patterns, and χ^2: goodness of fit indicator) of all samples sintered at 700–775 °C. Before sintering, the reagent powders were calcined at 650 °C to obtain the $Ce_2Zr_3(MoO_4)_9$ phase. The subsequent sintering at 700–775 °C is to promote sufficient grain growth as shown in the SEM results (Fig. 4). Normally, the cell parameters should maintain a stable value, but the refinement results show the lattice parameters and unit cell volumes at different sintering temperature change slightly, this maybe due to the lattice defects in the lattice. The value of all reliability factors are below 10%; χ^2 values are around 2.5, indicating that the results of the refinement are reliable. Fig. 2(e) exhibits the diagram of crystal structure. It can be seen that the Ce, Zr and Mo cations form oxygen polyhedra with 9, 6 and 4 oxygen ions, respectively. In addition, each MoO_4 polyhedron bridges two CeO_9 polyhedra and two ZrO_6 polyhedra through corner-sharing oxygen atom simultaneously. The length of the Zr–O bond and the oxygen polyhedral distortion (δ) are summarized in Table 2 based on the

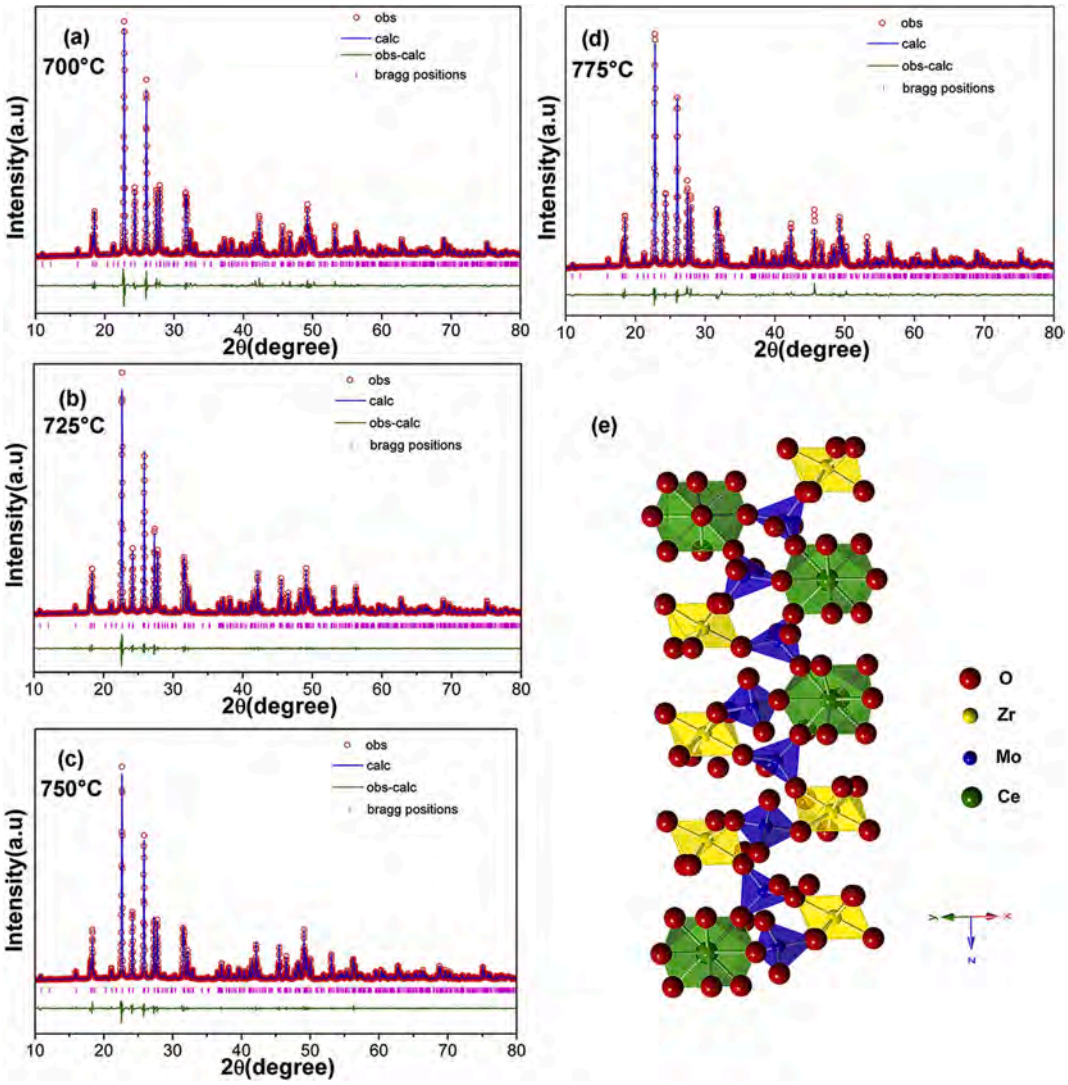

Fig. 2. Rietveld refinement patterns of the $Ce_2Zr_3(MoO_4)_9$ ceramics sintered at different temperature (a–d), and the crystal structure of $Ce_2Zr_3(MoO_4)_9$ (e).

Table 1
The refined lattice parameters, unit cell volume, and reliability factors of the $Ce_2Zr_3(MoO_4)_9$ ceramics sintered at different temperature. (S.T.: sintering temperature; V: unit cell volume.)

S.T.	a = b (Å)	c (Å)	V (Å^3)	Rwp (%)	Rp (%)	χ^2
700 °C	9.840298	58.887113	4938.185	7.27	5.33	2.55
725 °C	9.842139	58.894054	4940.615	7.20	4.93	2.54
750 °C	9.841748	58.888676	4939.722	7.05	4.89	2.33
775 °C	9.842671	58.895321	4941.206	7.75	5.73	2.68

Table 2
The bond length (R) and oxygen octahedral distortion (δ) of the $Ce_2Zr_3(MoO_4)_9$ at different temperature.

Type	S.T = 700 °C	S.T = 725 °C	S.T = 750 °C	S.T = 775 °C
$R_{Zr\text{-}O1} \times 3$	2.026	2.025	1.984	2.003
$R_{Zr\text{-}O2} \times 3$	2.154	2.097	2.08	2.190
$\overline{R}$	2.090	2.061	2.032	2.097
δ(%)	6.12	3.49	4.72	8.92

Table 3
Irreducible representations and the classification of Infrared and Raman active modes of $Ce_2Zr_3(MoO_4)_9$.

D_{3d}	E	$2C_3$	$3C_2$	i	$2S_6$	$3\sigma_d$	Selection rules
A_{1g}	1	1	1	1	1	1	$\alpha_{xx}+\alpha_{yy},\ \alpha_{zz}$
A_{2g}	1	1	−1	1	1	−1	R_z
E_g	2	−1	0	2	−1	0	$(R_x,R_y),(\alpha_{xx}-\alpha_{yy},\alpha_{xy}),(\alpha_{xz},\alpha_{yz})$
A_{1u}	1	1	1	−1	−1	−1	
A_{2u}	1	1	−1	−1	−1	1	T_z
E_u	2	−1	0	−2	1	0	(T_x,T_y)

results of the Rietveld refinement. The octahedral distortion can be calculated by the following equation [18].

$$distortion(\delta) = \frac{Zr-Odistance_{\max} - Zr-Odistance_{\min}}{Zr-Odistance_{average}} \quad (4)$$

Raman scattering spectrum is widely used to detect solid lattice vibration, which qualitatively and quantitatively reflects the microstructure, phase transition, impurities and defects of solids. $Ce_2Zr_3(MoO_4)_9$ ceramics are member of Trigonal system with R–3C space group (D_{3d}, No. 167). Based on the group theory and the symmetry analysis using the Bilbao Crystallographic Server, the total lattice vibrations of

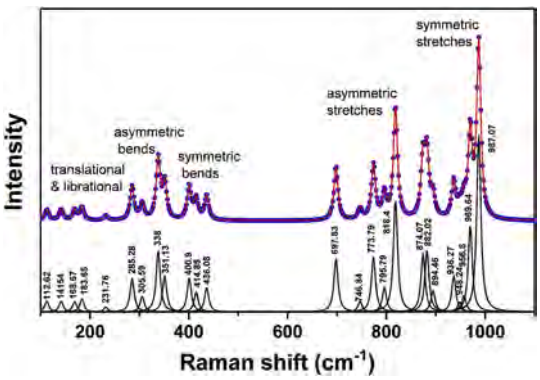

Fig. 3. Deconvoluted Raman spectra of the $Ce_2Zr_3(MoO_4)_9$ ceramics.

$Ce_2Zr_3(MoO_4)_9$ can be expressed as [19,20]:

$$\Gamma = 24A_{1g} + 25A_{1u} + 25A_{2g} + 25A_{2u} + 50E_u + 49E_g$$

And the irreducible representations of Raman and Infrared active modes are listed in Table 3. Notably, the selection rules of *T*and α represent the molecular translational vibration mode and rotational vibration mode respectively, which means that *T* is infrared activated mode and α is Raman activated mode. Therefore, 73 Raman peaks ($24A_{1g}$+$49E_g$) can be observed on the characteristic Raman spectrum.

However, due to the overlapping signals and the test limitation of the Raman spectra, only a few typical Raman peaks can be marked in the range of 100–1100 cm^{-1} as shown in Fig. 3. Compared to several similar MoO_4 tetrahedron in $PbMoO_4$, $CaMoO_4$, β- $Bi_2Mo_2O_9$ [21] and $Gd_2Zr_3(MoO_4)_9$, we can be determined that the intensive line in the range of 900–1100 cm^{-1} are caused by symmetric stretching, and the bands in the range of 750–900 cm^{-1} are assigned to asymmetric stretching, while several primary bands at 320-400 cm^{-1} and 280-320 cm^{-1} are corresponding to symmetric bending and asymmetric bending vibrations [19]. In addition, the intensive line below 280 cm^{-1} may attributed to the translational and librational motions of the Ce or Zr ions [22].

Fig. 4(a–d) shows the SEM micrographs of the cross sections of $Ce_2Zr_3(MoO_4)_9$ ceramics sintered at 700–775 °C for 4 h. Clear grain boundaries are observed for all samples. For the sample sintered at 700 °C and 725 °C, irregular grain shape and pores are detected. The statistical distribution of grain size is shown in Fig. 5, and the grain size reached to an optimal state at 750 °C as shown in Fig. 4(e). The relative density values (>92%) are obtained for all samples and exhibited in Fig. 4(f). It is observed that the relative density inclines first and reaches to an optimum value at 750 °C with the sintering temperature rising. However, further increasing of the sintering temperature reduces the relative density slightly, which is consistent well with the SEM results. Such phenomenon is probably due to the unexpected porosity caused by the mismatch between grain growth and grain boundary growth at high temperature.

Fig. 6(a) exhibits the dielectric constants and the Q × f values of the $Ce_2Zr_3(MoO_4)_9$ ceramics sintered at different temperature. The

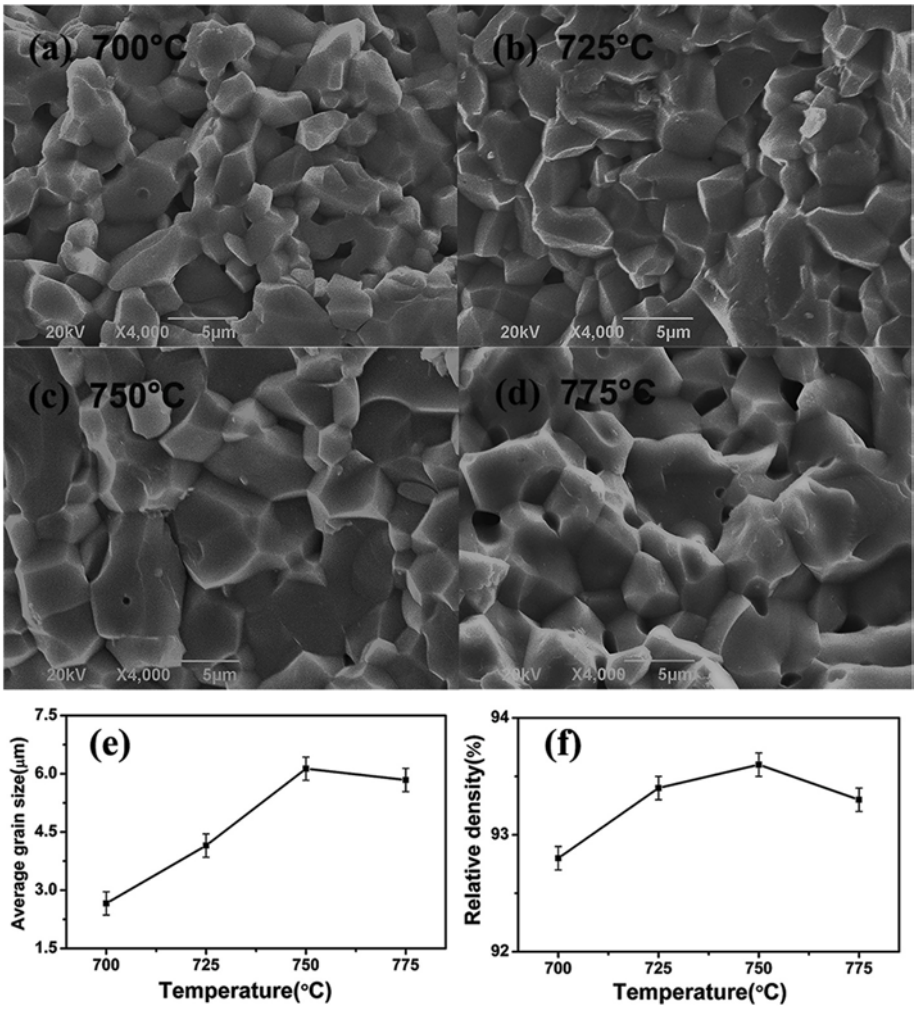

Fig. 4. SEM images (a–d), the average grain size (e), and the relative density (f) of the $Ce_2Zr_3(MoO_4)_9$ ceramics sintered at different temperature.

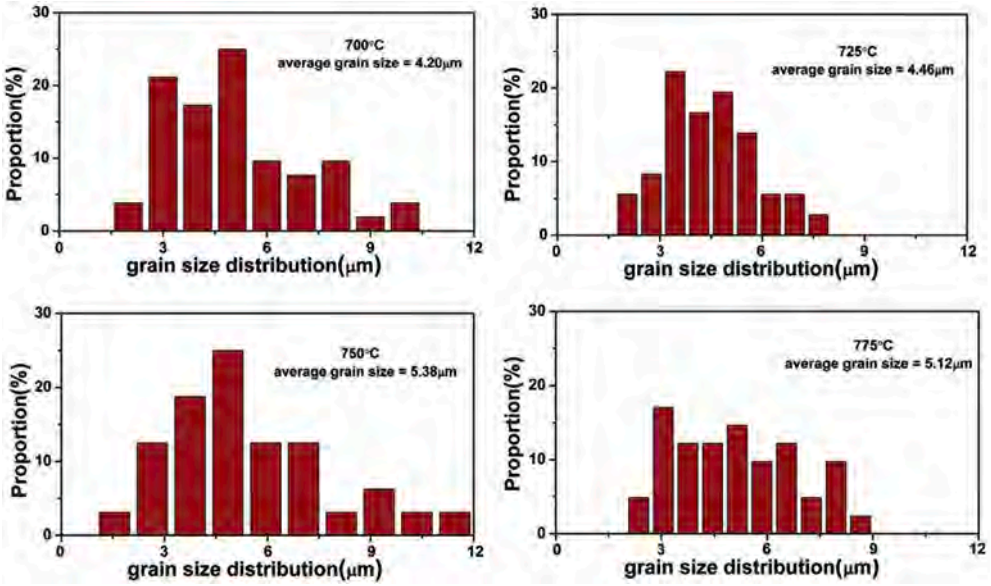

Fig. 5. The statistical distribution of grain size.

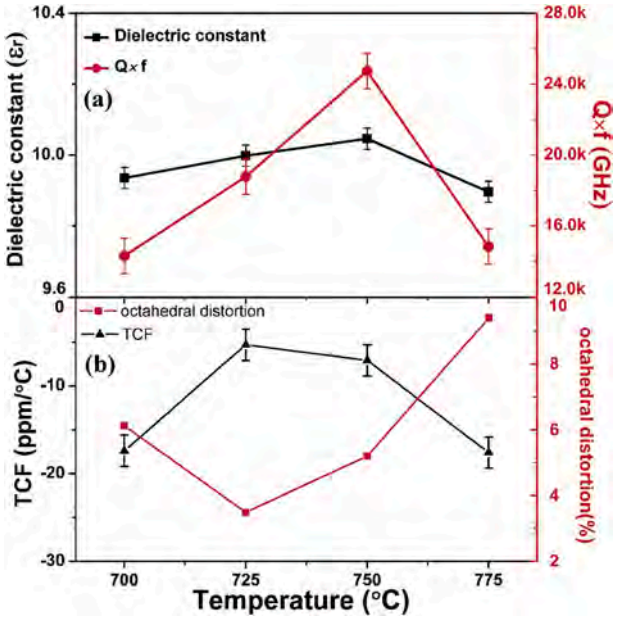

Fig. 6. Dielectric constant and Q × f values (a); temperature coefficient of resonant frequency and oxygen octahedral distortion values (b) at different temperature.

Table 4
The measured dielectric constant (ε_m), the porosity corrected dielectric constant (ε_{cv}), the porosity fraction (p), the Q × f values, and the packing fraction (P.F.) values of the $Ce_2Zr_3(MoO_4)_9$ ceramics sintered at different temperature.

S.T.	700 °C	725 °C	750 °C	775 °C
p	0.072	0.066	0.064	0.067
ε_m	9.935	9.998	10.050	9.896
ε_{cv}	10.964	10.939	10.960	10.841
Q × f (GHz)	14,300	17,182	24,740	15,360
P.F. (%)	53.229	53.203	53.212	53.196

dielectric constant value increases with the sintering temperature and reaches to a peak value of 10.05 at 750 °C. Then it decreases with further increasing the sintering temperature. The variation of ε_r value is similar to the tendency of the relative density. To further investigate the relationship between the dielectric constant and the density, we obtained the porosity corrected value of the dielectric constant by the following equation [23]:

$$\varepsilon_m = \varepsilon_{cv}\left[1 - \frac{3p(\varepsilon_{cv}-1)}{2\varepsilon_{cv}+1}\right] \quad (6)$$

where ε_m, ε_{cv}, and p represent the measured dielectric constant, the porosity corrected value of dielectric constant, and the porosity fraction, respectively. The ε_m, ε_{cv} and p are listed in Table 4. The corrected dielectric constant (~10.9) is greater than the measured values and remains unchanged essentially. In addition, the variation of the corrected dielectric constant is inverse to the change of the porosity fraction, suggesting that the dielectric constant is influenced by pores [24].

Generally, the microwave dielectric loss is largely affected by both internal and external factors. The external loss is mainly induced by porosity, density, and grain defects; while the internal loss mainly arises from the crystal structure [25,26]. The packing fraction (P.F.), as an effective internal factor, is usually adopted to study the influence of the internal and external loss impacts on the Q × f values, which is calculated by the following equation [27]:

$$P.F(\%) = \frac{volume\ of\ packed\ ions}{volume\ of\ primitive\ unite\ cell} \quad (7)$$

The calculated P.F. values and Q × f values are summarized in Table 4, which remain around 53.2%. It can be also observed that the variation of the Q × f value possesses a similar trend to the relative density, as shown in Fig. 3(f). This fact indicates that the dielectric loss of the as-sintered $Ce_2Zr_3(MoO_4)_9$ ceramics are also related to the external factors. Therefore, the Q × f value gradually increases and reaches to the maximum value of 24,720 GHz (at 11.3 GHz) at the sintering temperature of 750 °C, where the porosity stays at a lower value, as confirmed in Fig. 4(f). Further increasing of the sintering temperature results in a slightly decreased Q × f value due to the appearance of pores. Based on the packing and porosity fraction analysis, it is concluded that the Q × f values are not only affected by internal factors but also more affected by external factors.

Fig. 6(b) shows the variation of the τ_f values and oxygen polyhedral

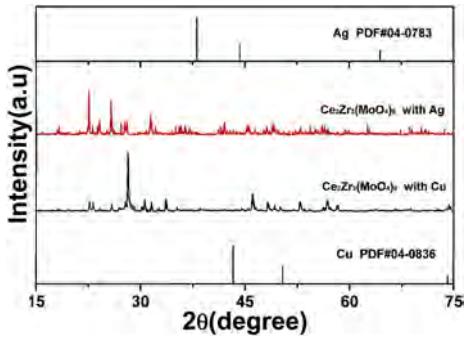

Fig. 7. XRD patterns of the $Ce_2Zr_3(MoO_4)_9$ ceramics co-fired with Cu and Ag at 750 °C.

distortion of the $Ce_2Zr_3(MoO_4)_9$ ceramics sintered at different temperature. The variation of the τ_f value is inverse to that of the Zr–O oxygen octahedral distortion, revealing that the temperature characteristics are largely affected by the octahedron distortion. Furthermore, the τ_f values for all samples are negative. An acceptable value of −7.1 ppm/°C is obtained at the sintering temperature of 750 °C, indicating a decent dielectric thermal stability.

Co-firing compatibility of microwave ceramics with metal-electrode is an important criterion for LTCC applications. In the current study, 20 wt % copper (Cu) and silver (Ag) were added into the $Ce_2Zr_3(MoO_4)_9$ ceramic powders, respectively. The mixed powder was sintered at 750 °C for 1h. The XRD results are exhibited in Fig. 7. Unexpectedly, the phase of Cu and Ag cannot be detected after sintering, indicating that the $Ce_2Zr_3(MoO_4)_9$ matrix can react with Cu and Ag. This phenomenon is mainly due to the fact that the sintering temperature of Ag_2MoO_4 (450 °C) and $CuMoO_4$ (550 °C) are lower than that of $Ce_2Zr_3(MoO_4)_9$ [28,29]. Therefore, the poor compatibility between Cu/Ag and $Ce_2Zr_3(MoO_4)_9$ ceramic matrix prohibits its application in LTCC processing. To solve the co-firing compatibility between molybdate ceramic materials and metal electrode, it is a feasible method to explore possible metal electrode materials. For example, the good compatibility between aluminum and $CuMoO_4$, as reported by Nina Joseph et al. [30], indicates that aluminum maybe a good candidate metal electrode for $Ce_2Zr_3(MoO4)_9$ ceramic matrix. Therefore, exploring possible metal electrode materials is the focus of follow-up research.

4. Conclusion

In this work, $Ce_2Zr_3(MoO_4)_9$ dielectric ceramics were synthesized via the traditional solid-state reaction method. Pure $Ce_2Zr_3(MoO_4)_9$ phase with dense morphology were obtained at low sintering temperature range of 700–775 °C for 4 h. Optimal microwave dielectric performances were obtained in the sample sintered at 750 °C: $\varepsilon_r = 10.05$, $Q \times f =$ 24,720 GHz (at 11.3 GHz), and $\tau_f = -7.1$ ppm/°C. The $Ce_2Zr_3(MoO_4)_9$ dielectric ceramics prepared has poor compatibility with Cu and Ag. Our experimental results suggest that the $Ce_2Zr_3(MoO_4)_9$ system has optimal microwave dielectric performances, but the poor compatibility between Cu/Ag and $Ce_2Zr_3(MoO_4)_9$ ceramic matrix makes Cu/Ag unable to be used as $Ce_2Zr_3(MoO_4)_9$ ceramic matrix electrode.

Acknowledgements

This work was supported by the National Natural Science Foundation of China (Grant No. 51672036), the National Key Scientific Instrument and Equipment Development Project (No.51827802), the Major Science and Technology Specific Projects of Sichuan Province (No. 2019ZDZX0026), and the Fundamental Research Funds for the Central Universities (Grant No. ZYGX2019J021).

References

[1] H.W. Chen, H. Su, H.W. Zhang, T.C. Zhou, B.W. Zhang, J.F. Zhang, X.L. Tang, Low-temperature sintering and microwave dielectric properties of $(Zn_{1-x}Co_x)_2SiO_4$ ceramics, Ceram. Int. 40 (2014) 14655–14659.
[2] S.E. Kalathil, U.A. Neelakantan, R. Ratheesh, Microwave dielectric properties of ultralow-temperature cofirable $Ba_3V_4O_{13}$ ceramics, J. Am. Ceram. Soc. 97 (2014) 1530–1533.
[3] C. Liu, L. Shi, Y. Lai, Y. Li, L. Jia, H. Su, J. Li, T. Wen, W. Ling, H. Zhang, B-site modification of $(Ba_{0.6}Sr_{0.4})TiO_3$ ceramics with enhanced diffuse phase transition behavior, Ceram. Int. 44 (2018) 8109–8115.
[4] S. Lei, H. Fan, W. Chen, Effects of $CaO–B_2O_3$ glass addition on the low-temperature sintering and cation ordering in $Sr_xLa_{(1-x)}Ti_xAl_{(1-x)}O_3$ ceramics, J. Alloys Compd. 632 (2015) 78–86.
[5] M.T. Sebastian, H. Jantunen, Low loss dielectric materials for LTCC applications: a review, Int. Mater. Rev. 53 (2008) 57–90.
[6] G. Wang, H. Zhang, C. Liu, H. Su, J. Li, X. Huang, G. Gan, F. Xu, Low temperature sintering and microwave dielectric properties of novel temperature stable $Li_3Mg_2NbO_6$-0.1TiO_2 ceramics, Mater. Lett. 217 (2018) 48–51.
[7] C. Liu, H. Zhang, H. Su, T. Zhou, J. Li, X. Chen, W. Miao, L. Xie, L. Jia, Low temperature sintering BBSZ glass modified $Li_2MgTi_3O_8$ microwave dielectric ceramics, J. Alloys Compd. 646 (2015) 1139–1142.
[8] B. Liu, Y.H. Huang, K.X. Song, L. Li, X.M. Chen, Structural evolution and microwave dielectric properties in $Sr_2(Ti_{1-x}Sn_x)O_4$ ceramics, J. Eur. Ceram. Soc. 38 (2018) 3833–3839.
[9] H. Zuo, X. Tang, H. Zhang, Y. Lai, Y. Jing, H. Su, Low-dielectric-constant $LiAlO_2$ ceramics combined with LBSCA glass for LTCC applications, Ceram. Int. 43 (2017) 8951–8955.
[10] E.K. Suresh, A.N. Unnimaya, A. Surjith, R. Ratheesh, New vanadium based $Ba_3MV_4O_{15}$ (M=Ti and Zr) high Q ceramics for LTCC applications, Ceram. Int. 39 (2013) 3635–3639.
[11] M.T. Sebastian, H. Wang, H. Jantunen, Low temperature co-fired ceramics with ultra-low sintering temperature: a review, Curr. Opin. Solid. St. M. 20 (2016) 151–170.
[12] L.X. Pang, G.B. Sun, D. Zhou, $Ln_2Mo_3O_{12}$ (Ln = La, Nd): a novel group of low loss microwave dielectric ceramics with low sintering temperature, Mater. Lett. 65 (2011) 164–166.
[13] W.Q. Liu, R.Z. Zuo, A novel low-temperature firable $La_2Zr_3(MoO_4)_9$ microwave dielectric ceramic, J. Eur. Ceram. Soc. 38 (2018) 339–342.
[14] B.J. Tao, C.F. Xing, W.F. Wang, H.T. Wu, Y.Y. Zhou, A novel $Ce_2Zr_3(MoO_4)_9$ microwave dielectric ceramic with ultra-low firing temperature, Ceram. Int. 45 (2019) 24675–24683.
[15] B.W. Hakki, P.D. Coleman, A dielectric resonator method of measuring inductive capacities in the millimeter range, IRE. Trans. Microw. Theory Tech. 8 (1960) 402–410.
[16] G. Wang, H. Zhang, F. Xu, X. Huang, Y. Lai, G. Gan, Y. Yang, J. Li, C. Liu, L. Jin, Investigation and characterization on crystal structure and enhanced microwave dielectric properties of non-stoichiometric $Li_{3+x}Mg_2NbO_6$ ceramics, Ceram. Int. 44 (2018) 20539–20544.
[17] R.F. Klevtsova, S.F. Solodovnikov, Y.L. Tushinova, B.G. Bazarov, L.A. Glinskaya, Z. G. Bazarova, A new type of mixed framework in the crystal structure of binary molybdate $Nd_2Zr_3(MoO_4)_9$, J. Struct. Chem. 41 (2000) 280–284.
[18] S.D. Ramarao, V.R.K. Murthy, Crystal structure refinement and microwave dielectric properties of new low dielectric loss $AZrNb_2O_8$ (A: Mn, Zn, Mg and Co) ceramics, Scripta Mater. 69 (2013) 274–277.
[19] H. Yang, S. Zhang, H. Yang, Y. Yuan, E. Li, $Gd_2Zr_3(MoO_4)_9$ microwave dielectric ceramics with trigonal structure for LTCC application, J. Am. Ceram. Soc. 103 (2020).
[20] R.P.B.D.L. Rousseau, S.P.S. Porto, Normal mode determination in crystals, J. Raman Spectrosc. 10 (1981) 253–290.
[21] F.D. Hardcastle, I.E. Wachs, Determination of molybdenum–oxygen bond distances and bond orders by Raman spectroscopy, J. Raman Spectrosc. 21 (1990) 683–691.
[22] J. Dhanya, E.K. Suresh, R. Naveenraj, R. Ratheesh, Structure and microwave dielectric properties of low temperature sinterable $NaR_5(MoO_4)_8$ (R = La, Pr, Nd, Sm) ceramics, J. Electron. Mater. 48 (2019) 4040–4049.
[23] S.J. Penn, N.M. Alford, A. Templeton, X.R. Wang, M.S. Xu, M. Reece, K. Schrapel, Effect of porosity and grain size on the microwave dielectric properties of sintered alumina, J. Am. Ceram. Soc. 80 (1997) 1885–1888.
[24] L.X. Pang, D. Zhou, W.G. Liu, Z.M. Qi, Z.X. Yue, Crystal structure and microwave dielectric behaviors of scheelite structured (1-x)$BiVO_4$-x$La_{2/3}MoO_4$ ($0.0 \leq x \leq 1.0$) ceramics with ultra-low sintering temperature, J. Eur. Ceram. Soc. 38 (2018) 1535–1540.
[25] Z. Fu, P. Liu, J. Ma, X. Zhao, H. Zhang, Novel series of ultra-low loss microwave dielectric ceramics: $Li_2Mg_3BO_6$ (B = Ti, Sn, Zr), J. Eur. Ceram. Soc. 36 (2016) 625–629.
[26] Y. Wang, T.L. Tang, J.T. Zhang, W.S. Xia, L.W. Shi, Preparation and microwave dielectric properties of new low-loss $NiZrTa_2O_8$ ceramics, J. Alloys Compd. 778 (2019) 576–578.
[27] C.H. Su, F.C. Lin, T.M. Chu, C.L. Huang, Structural characteristics and microwave dielectric properties of low-firing $Ba(Co_{1-x}Mg_x)_2(VO_4)_2$ (x=0–1) ceramics, J. Alloys Compd. 686 (2016) 608–615.

[28] N. Joseph, J. Varghese, M. Teirikangas, M.T. Sebastian, H. Jantunen, Ultra-low sintering temperature ceramic composites of $CuMoO_4$ through Ag_2O addition for microwave applications, Compos. B Eng. 141 (2018) 214–220.
[29] D. Zhou, W.B. Li, L.X. Pang, J. Guo, Z.M. Qi, T. Shao, Z.X. Yue, X. Yao, P.K. Davies, Sintering behavior and dielectric properties of ultra-low temperature fired silver molybdate ceramics, J. Am. Ceram. Soc. 97 (2014) 3597–3601.
[30] N. Joseph, J. Varghese, T. Siponkoski, M. Teirikangas, M.T. Sebastian, H. Jantunen, Glass-free $CuMoO_4$ ceramic with excellent dielectric and thermal properties for ultralow temperature cofired ceramic applications, ACS Sustain. Chem. Eng. 4 (2016) 5632–5639.